

Electrostatic Origin of Element Selectivity during Rare Earth Adsorption

Mitchell Miller,¹ Yihao Liang,² Honghao Li,^{1,2} Miaoqi Chu,¹ Sangjun Yoo,¹ Wei Bu,³
 Monica Olvera de la Cruz,^{1,2} and Pulak Dutta^{1,*}

¹*Department of Physics and Astronomy, Northwestern University, Evanston, Illinois 60208, USA*

²*Department of Materials Science and Engineering, Northwestern University, Evanston, Illinois 60208, USA*

³*Center for Advanced Radiation Sources, University of Chicago, Chicago, Illinois 60637, USA*

 (Received 10 September 2018; revised manuscript received 17 December 2018; published 8 February 2019)

Rare earths, which are fundamental components of modern technologies, are often extracted from aqueous solutions using surfactants at oil-water interfaces. Heavier lanthanides are more easily extracted, even though all lanthanides are chemically very similar. Using x-ray fluorescence measurements and theoretical arguments, we show that there is a sharp bulk-concentration-dependent transition in the interfacial adsorption of cations from aqueous solutions containing Er^{3+} or Nd^{3+} in contact with a floating monolayer. The threshold bulk concentration of erbium ($Z = 68$) is an order of magnitude lower than that of neodymium ($Z = 60$), and erbium is preferentially adsorbed when the solution contains both ions. This implies that elemental selectivity during separation originates at the surfactant interface. Electrostatic effects arising from the interface dielectric mismatch, ionic correlations, and sizes of the ions explain the sharp adsorption curve and selectivity.

DOI: [10.1103/PhysRevLett.122.058001](https://doi.org/10.1103/PhysRevLett.122.058001)

Lanthanides are rare earths used in high-tech applications [1–3], in medicine [4], and in biology [5]. The industrial process of solvent extraction, which is used in mining and refinement of rare earths, works by placing an aqueous solution containing lanthanide ions in contact with an oil phase, with amphiphiles (“extractants”) at the interface [1]. The ions are transferred from the aqueous solution to the oil phase during the process. Despite decades of research [2,3], there is very little understanding of fundamental aspects of this process. One example is the lanthanides’ nearly ubiquitous trend of increased extraction efficiency as a function of atomic number [1], in spite of the fact that all lanthanides have the same outer shell and are therefore chemically similar. While no experiments have identified the nanoscale origin of this selectivity, hypothesized explanations include metal hydration differences [6], and adsorption competition with other salts present in the solution [7]. The selectivity may be rooted in the “lanthanide contraction” [8], which is the decrease in ionic radii r of lanthanide atoms as the atomic number Z increases [9].

Indeed, the size of metallic multivalent ions is important in many phenomena, including the interaction between emulsions containing lanthanides dispersed in an oil phase [8,10], as well as their adsorption to oppositely charged floating monolayers where they induce Z -dependent lateral ordering [11]. Interestingly, at very low or zero monovalent salt concentration, LaCl_3 and other multivalent metallic salts induce a sharp transition in strongly charged polyelectrolytes [12] from an extended charged state to a collapsed electrically neutral ionic structure. This transition

is due to correlations that develop from the “condensation” (adsorption) of ions to the polyelectrolyte, which is a function of the ion size and the polyelectrolyte conformation [13,14], as observed in simulations of monovalent ions [15], of multivalent ions [16], and more recently in simulations that include the dielectric mismatch caused by ion condensation [17,18].

Using x-ray fluorescence near total reflection (XFNTR) [19] measurements, we have observed a sharp bulk-concentration-dependent transition in the interfacial adsorption of lanthanide ions from a solution in contact with an oppositely charged floating monolayer. We see an order of magnitude difference in bulk concentration at the adsorption thresholds of two lanthanides, Er^{3+} and Nd^{3+} , whose difference in ionic radius [9] is small: $r(\text{Nd}^{3+})/r(\text{Er}^{3+}) \approx 1.06$. The heavier lanthanide ion Er^{3+} adsorbs at lower bulk concentrations, consistent with the known higher extraction efficiency of heavier lanthanides. We have determined the conditions for such a sharp transition using Monte Carlo (MC) simulations. The observed sharp transition is explained by the dielectric mismatch at the interface as well as by ion-ion correlations. The adsorption selectivity is revealed in our model when the difference in lanthanide sizes is included.

We present the experimental results first. We used XFNTR to measure the interfacial number densities of two lanthanides, Er^{3+} and Nd^{3+} , adsorbed at floating monolayers of octadecylphosphonic acid (ODPA), as functions of their concentration in the bulk aqueous solution (unadjusted bulk $\text{pH} \sim 5.7$). The XFNTR method is described in Ref. [19], and details of our sample

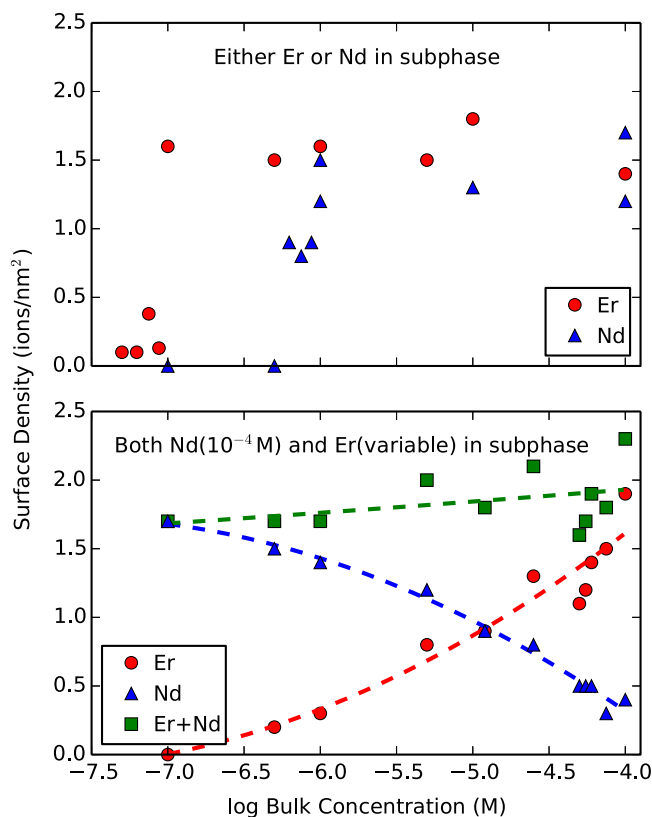


FIG. 1. Top: Surface density of lanthanide under the floating monolayer vs bulk concentration in the aqueous subphase, when there is only one lanthanide present (Er^{3+} or Nd^{3+}). In each case adsorption increases sharply at a threshold bulk concentration, but the threshold is an order of magnitude lower for Er^{3+} . Bottom: Surface densities of Er^{3+} and Nd^{3+} when the solution contains a mixture of the two lanthanides, and the Nd^{3+} concentration is fixed at 10^{-4} M while the Er^{3+} concentration is varied. The lines are polynomial fits, intended only as guides to the eye.

preparation and fluorescence measurements are in the Supplemental Material [20].

We first measured the interfacial lanthanide density when the only lanthanide in the aqueous subphase is Er^{3+} . With bulk solution concentrations above $\sim 5 \times 10^{-8}$ M of ErCl_3 , the surface density of erbium is roughly constant, at about 0.016 ions/ \AA^2 . However, at lower concentrations the surface density drops quite sharply to essentially zero. This is shown in Fig. 1 (top).

Nd^{3+} ions in solution likewise show an attraction to ODPa monolayers, but to a lesser extent (Fig. 1, top). The surface density at high bulk concentrations is roughly the same as that of Er^{3+} at equivalent concentrations, but at $\sim 5 \times 10^{-7}$ M NdCl_3 and below, the surface density decreases sharply to zero. Thus, the bulk concentration thresholds of these very similar ions differ significantly.

Mixtures of Nd^{3+} and Er^{3+} in aqueous solution were also studied. When there are equal above-threshold

concentrations (10^{-4} M of NdCl_3 and ErCl_3), there is 5 times as much Er^{3+} compared to Nd^{3+} at the interface (Fig. 1, bottom). When the Er^{3+} concentration is reduced while the Nd^{3+} concentration is constant, there is a continuous decrease in Er^{3+} surface density and a roughly equal increase in Nd^{3+} density (i.e., the total surface density is approximately constant). To achieve a 50% reduction in Er^{3+} surface density, the bulk Er^{3+} concentration must be lower than the bulk Nd concentration by an order of magnitude.

A previous report [11] showed that ODPa molecules have an area of ~ 0.21 nm² when spread over lanthanide salt solutions. In pure solutions, the data reported here mean that above the “steps” in Fig. 1, there are approximately three ODPa molecules for every lanthanide ion at the interface. When both cations are present in the subphase (Fig. 1, bottom), the total surface number density remains almost constant while the relative bulk concentrations are varied. Here again there is approximately 1 lanthanide ion per 3 ODPa molecules.

Neither the sharp jumps in the surface adsorption as a function of bulk concentration, nor the large difference in the surface adsorption thresholds of Er^{3+} and Nd^{3+} , are intuitive or easy to explain. However, they follow from the model we will now discuss. Since we are at an interface, we cannot assume a homogenous dielectric medium with an overall relative dielectric constant (ϵ_r). The dielectric environment changes dramatically in the vicinity of interface [21–23], and the presence of dissolved ions also results in a different bulk dielectric constant [24]. For example, at an interface between water ($\epsilon_{\text{water}} \approx 80$) and air ($\epsilon_{\text{water}} = 1$) the interaction between charges at the interface is governed by the mean dielectric media value ($\epsilon_{\text{water}} \approx 40$), and even when the head groups are charged and thus totally immersed in water, the concentration of charge is high enough to approach local molarity at which the water dielectric constant is highly reduced (e.g., $\epsilon_r \approx 45$ at $3M$ of NaCl [25]). Moreover, the electrostatic interactions are modified by the concentration of charged groups, including both the charge dissociated from the head groups of the amphiphiles and the charge of the adsorbed ions. Though full atom simulations are the best tool to study electrostatic interactions in systems with dielectric inhomogeneity, they lack a mechanism to dynamically change the degree of charge dissociation of molecules. Therefore, the adsorption of lanthanide ions under surfactant monolayers is determined here self-consistently by using Monte Carlo (MC) simulations [24] that account for the degree of charge dissociation near a surface [26]. Indeed, if one amphiphile dissociates near the interface, then due to the strong electrostatic repulsion between the neighboring charges, it will become harder for its immediate neighbors to dissociate. However, if one positively charged lanthanide ion is absorbed, it will be easier for nearby amphiphiles to dissociate. Therefore, the actual dissociation and adsorption rates depend on the range

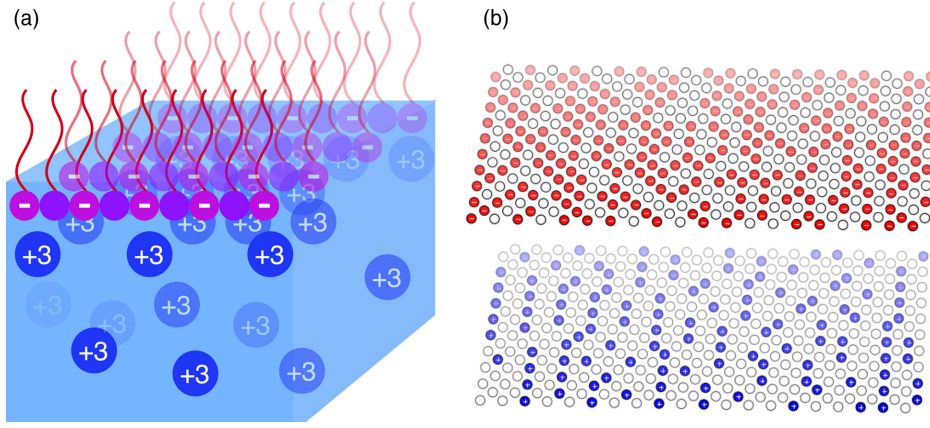


FIG. 2. (a) Schematic diagram of the system being simulated. (b) Sample Monte Carlo simulation setup (smaller 20×20 system shown here for clarity) in the model of two sharp interfaces separated by distance d_{inter} . The upper interface is in contact with air and the lower interface is in contact with water. The upper hexagonal lattice layer is the molecular monolayer and the lower hexagonal lattice layer is composed of lanthanides. Red indicates charged molecules, blue is adsorbed lanthanides, and white is neutral molecules (upper layer) or empty lanthanide sites (lower layer). The separation in the z direction (d_{inter}) is exaggerated here for clarity.

of electrostatic correlations, the dielectric environment, and the specific arrangement of amphiphiles and ions; see Fig. 2(a).

In order to use the MC lattice model [24] to determine the fraction of charge dissociated from the amphiphile head groups and the adsorption of ions, we choose hexagonal lattices for both ODPa molecules and lanthanide ions (i.e., we assume commensurability in lateral order, though the amphiphile lattice and the adsorbed multivalent ion lattice are not always commensurate [11]). One layer represents the ODPa molecule headgroups, while the other represents the lanthanide ions [Fig. 2(b)]. For the molecular layer, each site can have $-1e$ (dissociated) or 0 (neutral) charge; for the ionic layer, each site can have $+3e$ (adsorbed) or 0 (not adsorbed) charge. Two nearby sites are separated by $\sigma = 0.5$ nm, comparable to the size of hydrated ions. The distance between two layers d_{inter} is approximately the size of the hydrated lanthanide ions, which we set as $d_{\text{inter}} = \sigma$ for Er^{3+} and $d_{\text{inter}} = 1.07\sigma$ for Nd^{3+} , close to the reported Er^{3+} and Nd^{3+} size [9].

The MC model introduces several parameters to capture the dielectric inhomogeneity. The Bjerrum length $l_B = (e^2/4\pi\epsilon_0\epsilon_r k_B T)$, where ϵ_r is the relative permittivity of the medium, e is the unit charge, and $k_B T$ is the thermo energy, determines the strength of the screened electrostatic interaction between two charges separated by a distance r_{ij} , $(E/k_B T) = l_B(z_i z_j / r_{ij})e^{-\kappa r_{ij}}$, where z_i is the valence of the i species (amphiphile head group or lanthanide), and κ is the inverse of Debye screening length $\lambda_D = \kappa^{-1}$. Here, we assume λ_D is solely determined by the bulk salt concentration. To capture the dielectric inhomogeneity, we introduce l_B^+ , l_B^- , and l_B^{inter} , which represent the electrostatic strength of positively charged ion-ion interactions, negatively charged molecule-molecule interactions, and inter-layer molecule-ion interactions, respectively.

The Hamiltonian in our MC simulations is then given by

$$\frac{H}{k_B T} = -n_+ \ln(cV_0) + \frac{\mu}{k_B T} n_- - l_B^{\text{inter}} \sum_{+-} \frac{Z_+ Z_-}{r_{+-}} e^{-\kappa r_{+-}} + l_B^- \sum_{--} \frac{Z_- Z_-}{r_{--}} e^{-\kappa r_{--}} + l_B^+ \sum_{++} \frac{Z_+ Z_+}{r_{++}} e^{-\kappa r_{++}}, \quad (1)$$

where n_+ is the number of adsorbed ions (i.e., how many lattice sites have $+3$ charge), c is the bulk concentration of lanthanide ions, $\kappa = 4\sqrt{3\pi l_B c}$ with l_B the Bjerrum length of water in the bulk, and V_0 is the volume of each $+3$ ion [for Er^{3+} : $V_0 = (4\pi/3)(\sigma/2)^3$ and for Nd^{3+} : $V_0 = (4\pi/3)(1.07\sigma/2)^3$]. Here, \sum_{+-} is the summation over all charged ion-molecule pairs, and the chemical potential μ that controls the dissociation of acid molecules is a constant given by [4] $\mu/k_B T = -\ln 10(\text{pH} - \text{p}K_a)$.

This phenomenon cannot be described by “metalliclike bonding” adsorption models of point multivalent ions onto continuously charged surfaces [27]. In ionic systems, a nonzero size of the ions and discrete charge separations between charges are required to evaluate ionic correlations (as in the “ionic bonding” two-state thermodynamic model of collapsed polyelectrolytes due to multivalent ions [14]). Besides the ion size, we need to provide the values of l_B^i , $i = \text{inter}, +$ and $-$. Since the bulk concentration of ions is highly diluted, we set the bulk water value to $l_B^{\text{water}} = 0.7$ nm. Now, since the amphiphiles are close to the air-water boundary with $\epsilon_{\text{average}} \approx 40$, we assume their interaction is given by the mean dielectric constant between water and air, giving $l_B^- = 2l_B^{\text{water}}$ (as stated above, this rough approximation is reasonable since when the amphiphiles are charged they are in water with a highly decreased dielectric constant [25]). Simplified MC simulations of a small system size [$L^2 = (80\sigma)^2$] are used to provide

reasonable values for the simulation parameters. With the experimental threshold concentration for erbium we fit $l_B^+ = 1.769l_B^{\text{water}}$, $l_B^{\text{inter}} = 1.963l_B^{\text{water}}$, with $d_{\text{inter}}(\text{Er}^{3+}) = \sigma = 0.5$ nm, which are reasonable values given that the large interfacial charge concentration [25] requires $l_B^- \approx l_B^{\text{inter}}$, and geometry requires $l_B^+ > l_B^{\text{water}}$. Note that the interlayer interaction strength decreases with decreasing l_B^{inter} and/or increasing d_{inter} . Therefore, for Nd^{3+} , which saturates at higher concentrations, we set $d_{\text{inter}}(\text{Nd}^{3+}) = 1.07\sigma = 0.535$ nm (consistent with $\text{Er}^{3+}/\text{Nd}^{3+}$ radius difference of $\approx 6\%$) [9], leave l_B^+ unchanged, and vary l_B^{inter} from $1.963l_B^{\text{water}}$ to $1.93l_B^{\text{water}}$.

In order to demonstrate that the adsorption is described by a first order transition at a particular concentration of trivalent ions, c^* , we perform Monte Carlo simulation with H in Eq. (1) starting from two initial scenarios and fix λ_D to be independent of bulk concentration from 22σ to 16σ . In case I the surface before the adsorption of the multivalent ions is assumed to be fully charged, and in case II the initial surface charge is assumed to be zero. We find that the sharp transition concentration \tilde{c}_f for case I is 4 orders of magnitude lower than \tilde{c}_e for case II at $\lambda_D = 22\sigma$. As λ_D decreases the differences between the two sharp transition values decrease. Moreover, though case II shows a sharper transition, the sharpness of the transition decreases as λ_D decreases and at $\lambda_D = 16\sigma$ both cases display a continuous adsorption profile (see Fig. S1 in the Supplemental Material [20]), that is, the hysteresis disappears. These observations demonstrate that in order to observe a first order adsorption transition, long range electrostatic interactions are required, and at the experimental values of $\lambda_D \approx 200\sigma$, would expect an unphysically low \tilde{c}_f value for case I, supporting the assumption that the initial charge surface before the 3^+ ions are added is indeed zero and the experiments are best described by case II. The hysteresis is analyzed further by computing the constraint free energy

$$F(\hat{n}_+) = -k_B T \ln \left[\text{Tr}_{\{n_+ = \hat{n}_+\}} \exp \left(-\frac{H}{k_B T} \right) \right],$$

using the Wang-Landau algorithm [28] (see Supplemental Material [20] for details). The free energy landscapes $F(\hat{n}_+)$ between the two transition points \tilde{c}_e and \tilde{c}_f show two local stable macrostates \hat{n}_{+1} and \hat{n}_{+2} , separated by a large energy barrier that exponentially reduces the probability of changing from one macrostate to the other (see Fig. 3). Based on this observation we can define a point c^* between \tilde{c}_e and \tilde{c}_f where two local minima have same $F(\hat{n}_+)$ value, which is further demonstrated to be the concentration at first order transition. The constraint free energy can be further rewritten as

$$\frac{F(\hat{n}_+, \epsilon)}{k_B T} = \frac{F^*(\hat{n}_+)}{k_B T} - \epsilon \hat{n}_+,$$

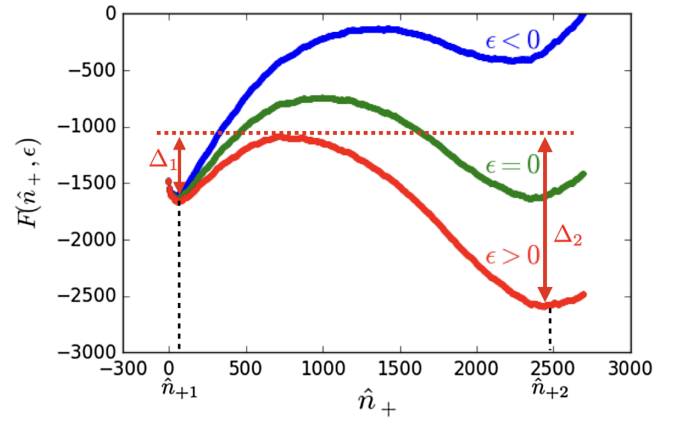


FIG. 3. Constraint free energy ($k_B T$) landscape of \hat{n}_+ near the concentration of the first order transition for Er^{3+} . These curves are obtained by the Wang-Landau algorithm, with $\lambda_D = 20\sigma$. The green curve corresponds to the transition point ($c^* = 10^{-9.17}$ M). The red curve corresponds to a higher bulk concentration $\epsilon > 0$ ($c = 10^{-9}$ M $> c^*$) and the blue curve to a lower bulk concentration $\epsilon < 0$, ($c = 10^{-9.4}$ M $< c^*$). The large values of energy barriers Δ_1 and Δ_2 imply hysteresis at this first-order transition.

where $F^*(\hat{n}_+) = -\ln[\text{Tr}_{\{n_+ = \hat{n}_+\}} \exp(-H^*/k_B T)]$, $\epsilon = \ln(c/c^*)$, and $H^* = H(c = c^*)$.

In the thermodynamic limit, $N \rightarrow \infty$, when $\epsilon > 0$ we obtain $F(\epsilon)/k_B T \approx \ln 2 - \epsilon \hat{n}_{+2}$, and when $\epsilon < 0$, $F(\epsilon)/k_B T \approx \ln 2 - \epsilon \hat{n}_{+1}$, which demonstrates that the transition is first order since $\hat{n}_{+1} < \hat{n}_{+2} \sim N$.

We obtained the adsorption curves for case II via MC simulations at various λ_D for Er^{3+} and Nd^{3+} . Though at $\lambda_D = 40\sigma$ the transition is sufficiently sharp (see Fig. S3 in the Supplemental Material [20]) we are not close to the experimental value of $\lambda_D = 200\sigma$, which requires simulations of exceedingly large system sizes. As mentioned earlier, the transition moves to lower values of \tilde{c}_e when increasing λ_D . Following the trends observed, we expect the shift to saturate to a \tilde{c}_e value (that is, larger λ_D will give the same \tilde{c}_e) for Er^{3+} at roughly $\tilde{c}_e \sim 10^{-11}$ (see Fig. S4 of the Supplemental Material [20]). Without polarization effects and keeping the same Bjerrum lengths, the largest $\lambda_D = 40\sigma$ simulated gives a difference in \tilde{c}_e between Er^{3+} and Nd^{3+} of about 0.06 orders of magnitude (see Figs. S3 and S4 of the Supplemental Material [20]). Moreover, when l_B^{inter} for Nd^{3+} decreases from $1.963l_B^{\text{water}}$ to $1.93l_B^{\text{water}}$, the transition threshold increases 0.78 orders of magnitude (see Figs. S3 and Fig. S4 of the Supplemental Material [20]). In total we can get 0.84 orders of magnitude difference in the transition concentration for Nd^{3+} and Er^{3+} . However, the values of \tilde{c}_e for both Er^{3+} and Nd^{3+} are too low. When the polarization is included [29] (see Fig. S5 of the Supplemental Material [20]) \tilde{c}_e moves to higher values at least by 2.4 orders of magnitude. Therefore, we expect the transition to be described by roughly the values of \tilde{c}_e at $\lambda_D = 40\sigma$ with an increase of at least 1.1 orders of

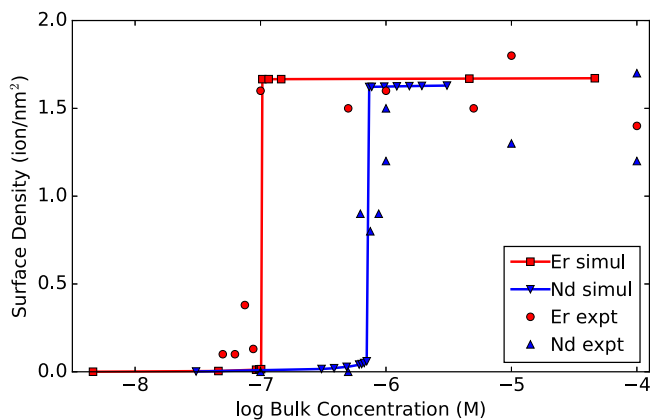


FIG. 4. Surface Er or Nd density vs bulk concentration determined by our MC simulations, overlaying the experimental data (same data as in Fig. 1, top). Since our simulations are for finite size systems, we cannot access experimental κ values; therefore, we shifted the simulation data from $\kappa^{-1} = 40\sigma$ to account for this effect and the polarization effect (see Supplemental Material [20] for details).

magnitude to account for both the fact that experimentally $\lambda_D = 200\sigma$ and the effect of the polarization.

The results of the simulation using $\lambda_D = 40\sigma$ and a system size of 200×200 are shown in Fig. 4. The conclusion is that a large screening length is required to obtain a first order transition and that the threshold concentration depends on the surface polarization (See Fig. S3 of the Supplemental Material [20]). Moreover, the vastly different threshold concentrations for Er^{3+} and Nd^{3+} are due to the different electrostatic interaction strengths resulting from their slightly different hydrated ion sizes and the changes in l_B^{inter} due to the confinement of the water in that region.

Clearly, full atom models [30] are required to validate the assumption of three different dielectric constants associated with l_B^i , $i = \text{inter}, +$ as well as MC simulations [31] that account for dielectric inhomogeneities [32] to compare with our results. However, full-atom potentials of hydration of trivalent metallic ions were only recently optimized [33] and more work is still needed to get interactions between the ions and the charged head groups. Therefore, this study provides a basis for further theoretical study of adsorption transitions reported in the experiments.

As shown in Fig. 1 (bottom), a mixture of Nd^{3+} and Er^{3+} does not show any sharp transition with increasing bulk concentration. From the computational point of view, the three-component system (Nd^{3+} , Er^{3+} , and OPA) is too complicated to obtain any simple physical insight. However, the simulations for the one component system show the transition becomes continuous when the screening length decreases (see Supplemental Material [20]), supporting the experimental results.

In summary, this study shows a strong elemental selectivity in the adsorption of dissolved rare earths at

amphiphile-containing interfaces. Electrostatic effects arising from the inhomogeneity of the interfacial medium, ionic correlations and small size differences between ions are responsible for the strong selectivity and for the observed sharp adsorption transitions. The transition, when occurring in very dilute solutions of multivalent cations and with no monovalent cations, is first order. It occurs when the surface charge is at a maximum and the adsorption of ions neutralizes the surface charge, reminiscent of the sharp transition of strongly charged chains in multivalent ions. This work shows the importance of including dielectric mismatch, ionic sizes and correlations in electrostatic models, and it unifies various models that account for these effects in different contexts to the ubiquitous problem of adsorption of multivalent metallic ions to charged amphiphiles.

Our study indicates that the known strong dependence of lanthanide extraction efficiency on atomic number originates at the surfactant interface, rather than in the bulk or in dynamic effects during the extraction process. We expect that a better understanding of the basic physics of these systems will help improve the methods and materials used in these commercially important processes, and that approaches such as that described in this Letter will be useful in studies of other systems involving ions at aqueous interfaces.

M. M., M. C., S. Y., and P. D. were supported by National Science Foundation (NSF), Grant No. DMR-1612876. Y. L., H. L., and M. O. were supported by NSF Grant No. DMR-1611076. The x-ray diffraction measurements were performed at ChemMatCARS (Sector 15, Advanced Photon Source), which is supported by the U.S. National Science Foundation, Grant No. CHE-1346572. The Advanced Photon Source is supported by the U.S. Department of Energy, Contract No. DE-AC02-06CH11357.

M. M. and Y. L. contributed equally to this work.

*Corresponding author.

pducta@northwestern.edu

- [1] F. Xie, T. A. Zhang, D. Dreisinger, and F. Doyle, *Miner. Eng.* **56**, 10 (2014).
- [2] B. Qiao, G. Ferru, M. Olvera de la Cruz, and R. J. Ellis, *ACS Central Sci.* **1**, 493 (2015).
- [3] J. Rey, S. Dourdain, L. Berthon, J. Jestin, S. Pellet-Rostaing, and T. Zemb, *Langmuir* **31**, 7006 (2015).
- [4] S. N. Misra, M. A. Gagnani, and R. S. Shukla, *Bioinorg. Chem. Appl.* **2**, 155 (2004).
- [5] N. C. Martinez-Gomez, H. N. Vu, and E. Skovran, *Inorg. Chem.* **55**, 10083 (2016).
- [6] K. L. Nash and J. C. Sullivan, in *Handbook of the Physics and Chemistry of the Rare Earths*, edited by K. Gschneidner, Jr. (Elsevier Science Publishers, Amsterdam, 1991), Vol. 15, p. 347.

- [7] K. L. Nash, *Solvent extraction and ion exchange* **11**, 729 (1993).
- [8] G. Ferru, B. Reinhart, M. K. Bera, M. Olvera de la Cruz, B. Qiao, and R. J. Ellis, *Chem. Eur. J.* **22**, 6899 (2016).
- [9] M. Duvail, R. Spezia, and P. Vitorge, *ChemPhysChem* **9**, 693 (2008).
- [10] M. Shen, H. Li, and M. Olvera de la Cruz, *Phys. Rev. Lett.* **119**, 138002 (2017).
- [11] M. Miller, M. Chu, B. Lin, W. Bu, and P. Dutta, *Langmuir* **33**, 1412 (2017).
- [12] M. Olvera de la Cruz, L. Belloni, M. Delsanti, J. P. Dalbiez, O. Spalla, and M. Drifford, *Chem. Phys.* **103**, 5781 (1995).
- [13] P. González-Mozuelos and M. Olvera de la Cruz, *J. Chem. Phys.* **103**, 3145 (1995).
- [14] F. J. Solis and M. Olvera de la Cruz, *J. Chem. Phys.* **112**, 2030 (2000).
- [15] M. J. Stevens and K. Kremer, *J. Chem. Phys.* **103**, 1669 (1995).
- [16] P. Y. Hsiao and E. Luijten, *Phys. Rev. Lett.* **97**, 148301 (2006).
- [17] F. Fahrenberger, O. A. Hickey, J. Smiatek, and C. Holm, *Phys. Rev. Lett.* **115**, 118301 (2015).
- [18] I. Nakamura and Z. G. Wang, *Soft Matter* **9**, 5686 (2013).
- [19] W. Bu, H. Yu, G. M. Luo, M. K. Bera, B. Y. Hou, A. W. Schuman, B. H. Lin, M. Meron, M. I. Kuzmenko, M. R. Antonio, L. Soderholm, and M. L. Schlossman, *J. Phys. Chem. B* **118**, 10662 (2014).
- [20] See Supplemental Material at <http://link.aps.org/supplemental/10.1103/PhysRevLett.122.058001> for details of sample preparation, XFTR measurements, and simulations.
- [21] A. Schlaich, E. W. Knapp, and R. R. Netz, *Phys. Rev. Lett.* **117**, 048001 (2016).
- [22] D. J. Bonthuis, S. Gekle, and R. R. Netz, *Phys. Rev. Lett.* **107**, 166102 (2011).
- [23] Y. Levin, A. P. Dos Santos, and A. Diehl, *Phys. Rev. Lett.* **103**, 257802 (2009).
- [24] R. R. Netz, *J. Phys. Condens. Matter* **15**, S239 (2002).
- [25] B. Hess, C. Holm, and N. van der Vegt, *Phys. Rev. Lett.* **96**, 147801 (2006).
- [26] C. Y. Leung, L. C. Palmer, B. F. Qiao, S. Kewalramani, R. Sknepnek, C. J. Newcomb, M. A. Greenfield, G. Vernizzi, S. L. Stupp, M. J. Bedzyk, and M. Olvera de la Cruz, *ACS Nano* **6**, 10901 (2012).
- [27] I. Rouzina and V. A. Bloomfield, *J. Phys. Chem.* **100**, 9977 (1996).
- [28] F. Wang and D. P. Landau, *Phys. Rev. Lett.* **86**, 2050 (2001); *Phys. Rev. E* **64**, 056101 (2001).
- [29] J. Jackson, *Classical Electrodynamics* (Wiley, New York, 1975), pp. 147–149.
- [30] F. Fahrenberger, Z. Xu, and C. Holm, *J. Chem. Phys.* **141**, 064902 (2014).
- [31] P. Qin, Z. Xu, W. Cai, and D. Jacobs, *Commun. Comput. Phys.* **6**, 955 (2009).
- [32] A. C. Maggs and V. Rossetto, *Phys. Rev. Lett.* **88**, 196402 (2002).
- [33] B. F. Qiao, S. Skanthakumar, and L. Soderholm, *J. Chem. Theory Comput.* **14**, 1781 (2018).